Surface atomic structure of epitaxial LaNiO_{3} thin films studied by in situ LEED-I(V)

J. P. Ruf, P. D. C. King, V. B. Nascimento, D. G. Schlom, and K. M. Shen

Phys. Rev. B **95**, 115418 — Published 15 March 2017

DOI: 10.1103/PhysRevB.95.115418

Surface atomic structure of epitaxial $LaNiO_3$ thin films studied by *in situ* LEED-$I(V)$

J. P. Ruf,[1] P. D. C. King,[1,2] V. B. Nascimento,[3] D. G. Schlom,[2,4] and K. M. Shen[1,2]

[1] *Department of Physics, Laboratory of Atomic and Solid State Physics, Cornell University, Ithaca, NY 14853, USA*
[2] *Kavli Institute at Cornell for Nanoscale Science, Ithaca, NY 14853, USA*
[3] *Departamento de Física, ICEx-UFMG, CP 702, Belo Horizonte, MG CEP 30123-970, Brazil*
[4] *Department of Materials Science and Engineering, Cornell University, Ithaca, NY 14853, USA*

(Dated: February 21, 2017)

We report *in situ* low-energy electron diffraction intensity versus voltage (LEED-$I(V)$) studies of the surface atomic structure of epitaxially grown $(001)_{\rm pc}$-oriented (pc = pseudocubic) thin films of the correlated $3d$ transition-metal oxide $LaNiO_3$. Our analysis indicates the presence of large out-of-plane bucklings of the topmost LaO layers but only minor bucklings of the topmost NiO_2 layers, in close agreement with earlier surface x-ray diffraction data. In view of materials design approaches that have suggested using atomic-scale polar structural distortions to produce designer electronic structures in artificial nickelate heterostructures, we propose that the broken inversion symmetry inherent to the surface of rare-earth nickelate thin films offers a similar opportunity to study the coupling between atomic structure and electronic properties in this family of materials.

I. INTRODUCTION

The electronic properties of many quantum materials are extremely sensitive to subtle changes in their crystal structure. For example, the two-dimensional ruthenates $Sr_{2-x}Ca_xRuO_4$ can be tuned from spin-triplet superconductor, to metamagnetic metal, to antiferromagnetic insulator by sterically inducing tilts and rotations of the RuO_6 octahedral network[1]. Rare-earth nickelates $(RNiO_3)$[2] and manganites $(R_{1-x}(Sr,Ca)_xMnO_3)$[3] also display rich phase diagrams in the bulk, showing a variety of thermally driven metal-insulator transitions to spin-, charge-, and/or orbitally-ordered ground states by modifying the metal-oxygen bond lengths and angles. Recently, this has led to a significant research effort investigating how electronic and magnetic properties can be artificially controlled in thin films and heterostructures by controlling the crystal structure through knobs such as epitaxial strain and dimensionality[4–6].

Relaxation or reconstruction at heterointerfaces can also significantly impact the electronic and magnetic properties of atomically thin correlated materials[7,8], but an accurate determination of the atomic structure near the film-vacuum interface remains a challenge. Grazing incidence x-ray diffraction and low-energy electron diffraction intensity versus voltage (LEED-$I(V)$) have proven to be among the most reliable techniques for quantitative surface structural determination[9–11]. One advantage of LEED-$I(V)$ is that it can be performed in a standard laboratory setting on an uncontaminated, pristine sample surface, and can be readily integrated with high-vacuum thin-film deposition systems such as molecular beam epitaxy (MBE), without the need for synchrotron radiation.

In this work, we utilize LEED-$I(V)$ to perform structural refinements of the surface atomic structure of epitaxial thin films of $LaNiO_3$ grown by MBE. By benchmarking our results against measurements obtained by COherent Bragg Rod Analysis (COBRA) of synchrotron-based surface x-ray diffraction data[12], we demonstrate the strong sensitivity of LEED-$I(V)$ to structural distortions and its potential as a flexible, *in situ* tool to accurately determine the surface atomic structure of epitaxial thin films of complex materials, especially in situations where a polar discontinuity could dramatically alter the surface electronic structure[13,14].

II. METHODS

A. Experimental Details

Epitaxial thin films of $LaNiO_3$ were synthesized on $(001)_{\rm pc}$-oriented $LaAlO_3$ substrates using reactive oxide molecular beam epitaxy at 10^{-5} Torr of distilled ozone (80% O_3) at a substrate temperature of 550° C, following the procedures detailed in Ref. 15. Reflection high-energy electron diffraction oscillations during film growth, step-terrace topography observed by *ex situ* atomic force microscopy, and Kiessig fringes in x-ray diffraction scans all confirmed the presence of flat film-substrate and film-vacuum interfaces[15]. Immediately following growth, films were transferred under UHV to an analysis chamber with a base pressure of 5×10^{-11} Torr equipped with a four-grid LEED optics (SPECS ErLEED 150).

A typical LEED pattern recorded in reflection geometry at an incident beam energy of 140 eV for a ten monolayer (ML) $LaNiO_3$ film at 35 K is shown in Fig. 1a. For convenience, we index the LEED spots in terms of pseudocubic (h,k) coordinates where the $\hat{x}$ (horizontal) and $\hat{y}$ (vertical) directions are parallel to the Ni-Ni nearest-neighbor directions. In this coordinate system, the net in-plane momentum transfer of each spot equals $\vec{q} = 2\pi(h\hat{x} + k\hat{y})/a_{\rm pc,LaAlO_3}$, where $a_{\rm pc,LaAlO_3} = 3.791$ Å. To collect a full data set suitable for LEED-$I(V)$ analysis, similar images were acquired between 50 and 500 eV in energy steps of between 1 and 2 eV with an 8-bit digital CCD and analyzed following the methods of Ref. 16. Figure 1b shows the

unnormalized raw data plotted versus incident energy (horizontal axis) and scattering angle parallel to the direction through momentum-transfer space indicated by the red lines (vertical axis). For subsequent comparisons with theoretical calculations (Sec.II B), spot intensities were normalized to the incident beam current and averaged over symmetrically equivalent Bragg peaks to obtain 14 inequivalent $I(V)$ curves, for $(h,k)_{\rm pc}$ = $(1,0)$, $(1,1)$, $(\frac{3}{2},\frac{1}{2})$, $(2,0)$, $(2,1)$, $(\frac{5}{2},\frac{1}{2})$, $(2,2)$, $(\frac{5}{2},\frac{3}{2})$, $(3,0)$, $(3,1)$, $(3,2)$, $(4,0)$, $(4,1)$, and $(3,3)$, covering a total energy range of $E_{\rm total} = 2850$ eV. Finally, all $I(V)$ curves were smoothed using a weighted five-point cubic polynomial algorithm.

B. Structural Analysis by LEED-$I(V)$

To generate the simulated $I(V)$ curves necessary for LEED-$I(V)$ analysis, we used the symmetrized automated tensor LEED package (SATLEED)[17], with partial-wave phase shifts calculated using the optimized muffin-tin (MT) potential method[18]. The optimized MT method allowed for the inclusion of an energy-dependent real component $\mathrm{Re}[V_0(E)]$ of the inner potential in the subsequent analysis[19], which has been shown to be important for avoiding systematic errors in the surface structural determination of complex oxides[20,21]. All of our simulations employed a constant imaginary component of the inner potential $\mathrm{Im}[V_0] = -5$ eV and a total of ten phase shifts, which we found to be sufficiently accurate for the energy range studied here. Structural refinements started with isotropic vibrational amplitudes corresponding to the Debye temperatures reported by neutron powder diffraction measurements on bulk samples[2], and then adjusted the vibrational amplitudes in the final theory-experiment comparison so as to minimize the Pendry reliability factor, R_P.

Sharp diffraction spots in LEED are shown in Fig. 1a, indexed according to the pseudocubic real-space and reciprocal-space unit cells indicated by blue lines. In bulk, $LaNiO_3$ adopts a rhombohedral crystal structure (space group #167, $R\bar{3}c$, corresponding to an $a^-a^-a^-$ octahedral rotation pattern in Glazer notation), but under the biaxial strain imposed by the substrate, the symmetry is reduced to monoclinic (space group #15, $C2/c$, $a^-a^-c^-$). The primitive real-space surface unit cell for the latter structure (outlined in purple in Fig. 1) is $(\sqrt{2}\times\sqrt{2})R45^\circ$ relative to the pseudocubic surface unit cell; hence, Bragg peaks with half-integer h and half-integer k are not expected to be systematically extinct in our labeling scheme, as evidenced by spots outlined with red circles in Fig. 1a. By contrast, at all energies covered in our study, we did not observe the fractional beams $(h,k)_{\rm pc} = (\pm 1/2, \pm 1/2), (\pm 3/2, \pm 3/2), ..., (\pm n + 1/2, \pm n + 1/2)$ $n \in \mathbb{Z}$ at normal incidence; several representative positions are indicated by red squares in Fig. 1a. Since these spots were apparent in off-normal scattering geometries, we concluded that the plane group symmetry of the film surface must be either $p4gm$ or $p2gg$, with the glide reflection axes defined by the black dashed lines in Fig. 1a [23].

Assuming no ordered surface adsorbate layer(s) and a stoichiometric film, we arrived at the model for the surface crystal structure shown in Fig. 1c and 1d. Notably, although the translational symmetry of this model is compatible with a (1×1) termination of the $a^-a^-c^-$ atomic structure reported for the bulk of $LaNiO_3$ thin films strained to $LaAlO_3$[22], the presence of two perpendicular glide reflection axes is not: an ideal bulk-truncated $a^-a^-c^-$ structure would have just one glide reflection axis running parallel to the monoclinic c axis c_M (plane group pg), in which long-range ordered a^-a^- tilts of the oxygen octahedral network break the other glide reflection axis symmetry parallel to b_M. More generally, the polar discontinuity drawn schematically in Fig. 1d should be expected to induce sizable structural relaxations perpendicular to the film-vacuum interface that might suppress the a^-a^- tilting mode near the surface[21]; analysis of diffraction intensities is essential to characterize the intra-unit-cell electron density and thereby resolve any such deviations from the bulk structure. Owing to the four-fold rotational symmetry of the diffraction pattern, the $p2gg$ structure, if realized, must have equally populated 90°-rotated domains over the spot size of the incident electron beam ($\approx$ 1 mm), with a splitting of the rectangular unit cell dimensions a, b of less than a few percent—*i.e.*, $|b/a - 1| < 0.02 - 0.03$—otherwise the angular resolution of our LEED instrument would have allowed identification of distinct spots from separate domains.

III. RESULTS

We refined the structure in the LEED-$I(V)$ analysis by allowing the atomic positions in the top two monolayers of $LaNiO_3$ to relax, with lower layers fixed to the bulk structure reported for $LaNiO_3$ films on $LaAlO_3$[22]. Due to the surface sensitivity of LEED, any possible distortions below the top two monolayers have a negligible effect on the $I(V)$ curves. This leaves 20 atoms in the surface slab and 10 (12) independent atomic positional parameters to be refined by the model in $p4gm$ ($p2gg$) symmetry: four for the out-of-plane positions of La, apical O, Ni, and equatorial O plus one (two) for the in-plane displacement(s) of equatorial O per monolayer. In addition to these 10 (12) independent structural parameters, we also allowed the constant, energy-independent component of $\mathrm{Re}[V_0(E)]$ to vary within the tensor LEED search. Figures 2, 3, and 4 summarize the results of our LEED-$I(V)$ refinement for the surface structure of our 10 ML $LaNiO_3$ film. The minimum overall R-factor achieved for an LaO-terminated surface with $p4gm$ symmetry was $R_P = 0.26$, generally considered acceptable for LEED-$I(V)$ refinements, whereas NiO_2-terminated surfaces yielded significantly worse agreement, $R_P > 0.65$.

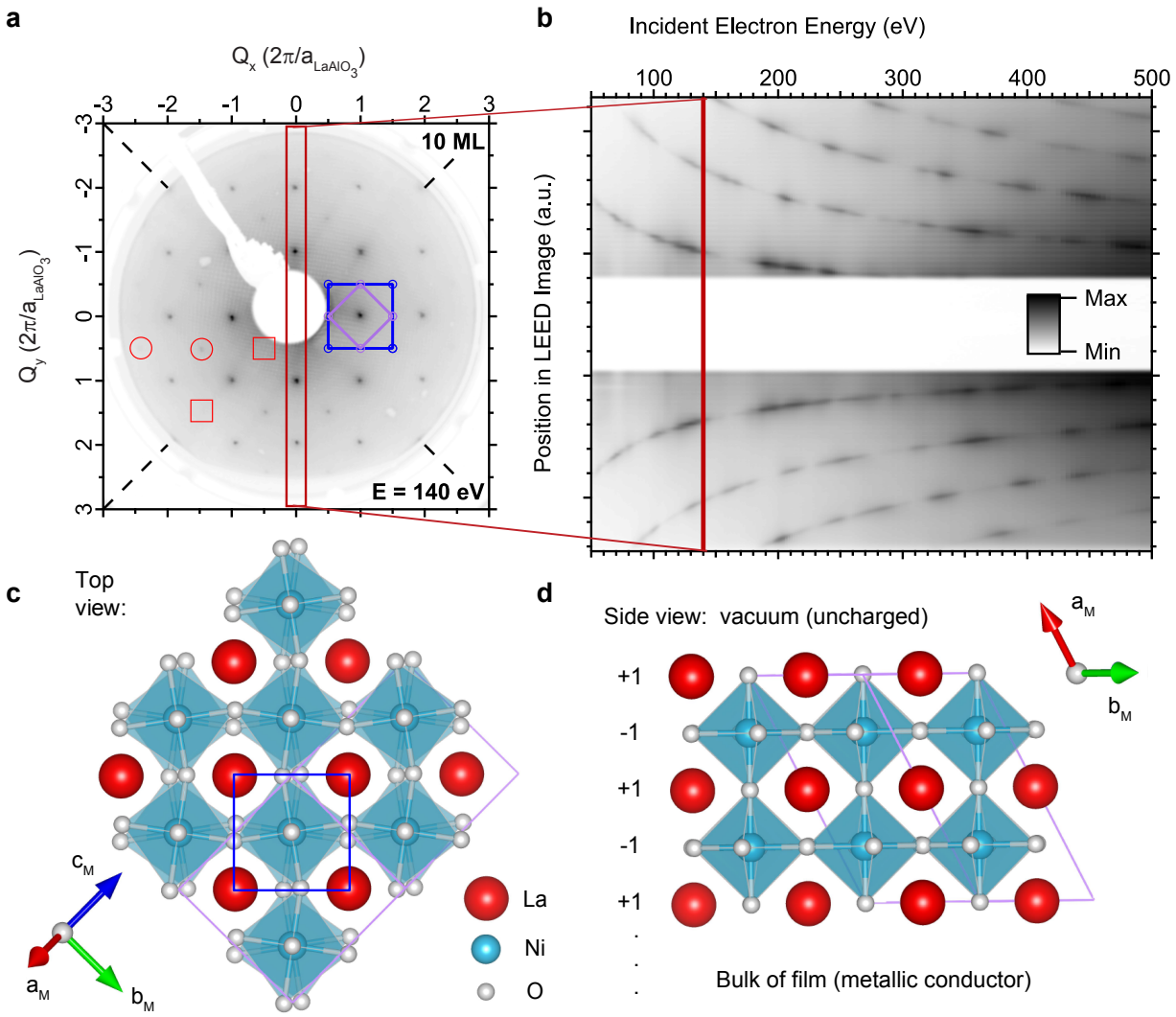

Figure 1. (a) LEED pattern of a 10 ML $LaNiO_3$ film/$LaAlO_3$ substrate recorded at an incident energy of 140 eV. Characteristic half-order positions where spots are (1) observed and (2) systematically extinct at normal incidence are outlined in (1) red circles and (2) red squares, respectively, indicating the presence of glide reflection axes parallel to the dashed black lines. (b) Experimental LEED intensity distributions parallel to the one-dimensional cut through momentum-transfer space indicated by the red box in (a), plotted versus incident electron energy. (c, d) Top and side views of the model used in subsequent structural refinements, following Ref. 22. The pseudocubic (monoclinic) real-space unit cells are outlined in blue (purple), corresponding to the primitive reciprocal space cells drawn in (a), with the orientation of the monoclinic crystal structure indicated by the $\{a_M, b_M, c_M\}$ triads. The electrostatic boundary conditions of the $(001)_{\mathrm{pc}}$-oriented film + vacuum interface are displayed schematically in (d) which, combined with the alternating $\pm 1e^-$ formal charges of the LaO and NiO_2 planes, necessitates atomic and electronic reconstruction at the film surface.

Models with $p4gm$ and $p2gg$ symmetry generally showed nearly equal R_P despite the two additional fitting parameters in the latter case, so we focus on the simpler $p4gm$ structures in the following analysis.

Experimental and simulated $I(V)$ curves for the best-fit structural model for a series of eight Bragg peaks are displayed in Fig. 2, and the numerical parameters of the best-fit model are summarized in the table in Fig. 3, along with the values for a bulk-truncated $LaNiO_3$ film on $LaAlO_3$[22]. To estimate the statistical errors in the model parameters, we took $\Delta R_P = R_{P,\,\mathrm{min}}\sqrt{8|\mathrm{Im}[V_0]|/E_{\mathrm{total}}} = 0.03$ as the uncertainty in the total R_P[24] and evaluated what uncorrelated displacements of each model parameter would cause deviations in R_P of this magnitude. Examining the table in Fig. 3, we note that large polar distortions of the LaO layers near the film-vacuum interface are essential for explaining the experimental data. This is expected, since $LaNiO_3$ along the $(001)_{\mathrm{pc}}$ direction is formally (in an ionic picture) a polar structure, with alternating $(LaO)^{+1}$ and $(NiO_2)^{-1}$

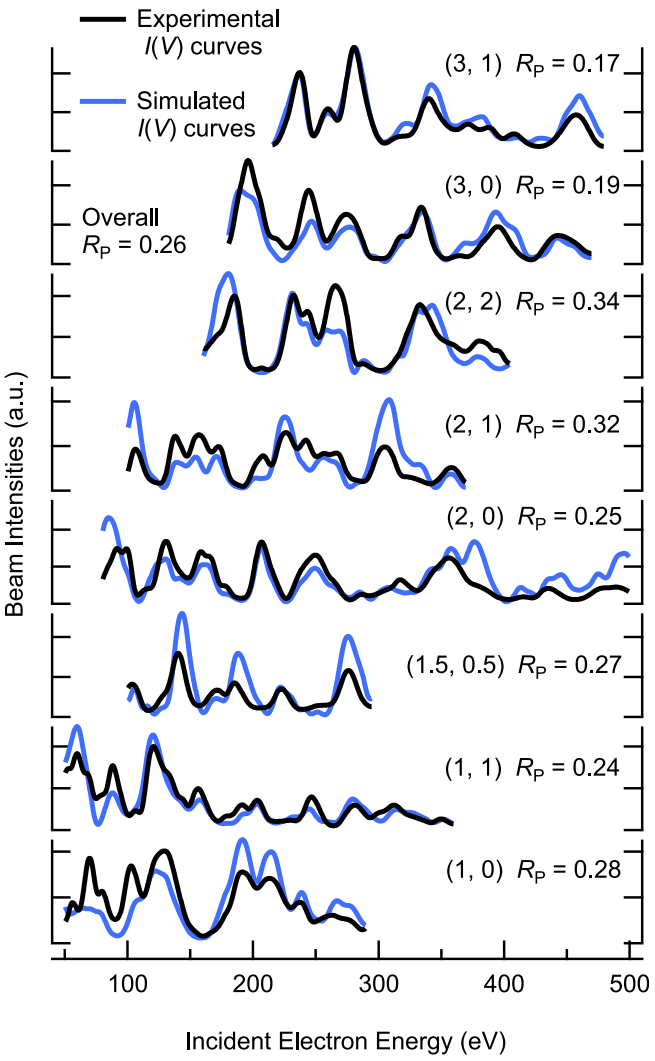

Figure 2. Comparison between experimental and theoretical LEED-$I(V)$ curves for the best-fit structure. Results for eight of the 14 beams used in the full structural refinement are shown, each labeled with their pseudocubic $(h,k)_{\rm pc}$ indices as described in the main text and the Pendry reliability factor R_P for that beam. The total R_P for the best-fit structure is 0.26 ± 0.03.

layers whose terminating interfaces are unstable towards structural and electronic reconstruction. The large bucklings of the topmost LaO layers, forming counter dipoles, are one pathway to resolving the polar discontinuity at the film-vacuum interface. On the other hand, the adjacent NiO_2 layers remain considerably flatter, and possess the same structure of the NiO_2 layers in bulk $LaNiO_3$ films to within the resolution of the LEED-$I(V)$ analysis. In the table we also show corresponding atomic displacements as determined from an earlier, separate COBRA analysis of surface x-ray diffraction of 3 ML $LaNiO_3$ thin films deposited on $LaAlO_3$ substrates by MBE, from Kumah *et al.*[12]. Remarkably, every relevant atomic coordinate of the first two unit cells agrees quantitatively, at least within the statistical uncertainty of the LEED-$I(V)$ analysis. That these two independent measurements agree so well strongly reinforces the validity of the LEED-$I(V)$ approach, and supports the correct determination of the surface structure of these $LaNiO_3$ thin films.

To demonstrate that the $I(V)$ curves depend sensitively on the out-of-plane bucklings in the topmost layer, we show in Fig. 4a a contour plot of R_P as a function of the displacements $\Delta z_{\rm La\text{-}1}$ (vertical axis) and $\Delta z_{\rm apO\text{-}1}$ (horizontal axis) away from their bulk values of zero in the upper right corner of the plot (corresponding to a flat terminating LaO plane). Positive z indicates displacement towards the interior of the film, away from vacuum. The existence of a deep, well-defined minimum in R_P near $\Delta z_{\rm La\text{-}1} = 0.23$ Å, $\Delta z_{\rm apO\text{-}1} = -0.18$ Å lends confidence in the reliability of the best-fit model. To directly illustrate the effects of changing these parameters, we calculated $I(V)$ curves for the $(h,k)_{\rm pc} = (1,1)$ beam for four different model structures indicated by differently colored dots/lines in Fig. 4, to be compared with the experimental data plotted in black in Fig. 4b. Clearly the lowest R_P structure reproduces the peaks and troughs of the experimental spectrum with reasonable fidelity, whereas the other structures with higher R_P have shifted in energy—or even miss—many of the experimentally measured features.

IV. DISCUSSION

The electron diffraction measurements and analysis presented above probe the ordered component of the atomic structure at the film-vacuum interface. Films were synthesized, transferred, and measured under UHV conditions without deliberate introduction of residual gases—*e.g.*, CO or $H_2O/H^+ + OH^-$—so adsorption of atoms or molecules onto the film surface are unlikely to form an overlayer(s) with long-range order; rather, any such chemical disorder probably contributes primarily to the intensity of the diffuse background that we subtract from the more rapidly varying intensity modulations in the $I(V)$ curves. We also simulated $I(V)$ curves for numerous non-stoichiometric surface structures, such as a double LaO termination[25,26], but none of these models were able to produce an $R_P < 0.6$.

While we cannot completely exclude the possibility of more complex surface structures stabilized by some combination of ordered oxygen and/or cation vacancies, as observed in the polar (001) surface of magnetite[27], we speculate that partial occupation of the atomic sites is the most likely deviation of the actual surface compared with the idealized model crystal structure drawn in Fig. 3. The best-fit model in our LEED-$I(V)$ simulations was obtained for Debye-Waller vibrational amplitudes of topmost La and apical O enhanced by a factor of ≈ 3 relative to their values in bulk $LaNiO_3$, which could be

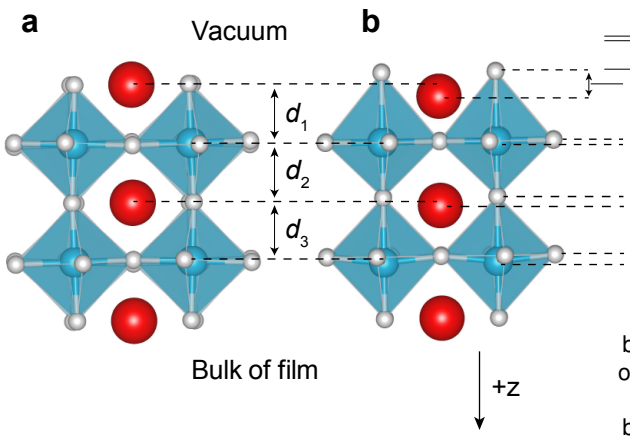

	(a)	(b)	
	Bulk, XRD	10 ML, LEED-$I(V)$	3 ML, COBRA
$\Delta z_{\text{LaO-1}}$	0.00 Å	0.41 ± 0.06 Å	0.37 Å
d_1	1.95 Å	1.90 ± 0.04 Å	—
$\Delta z_{\text{NiO}_2\text{-1}}$	± 0.05 Å	0.02 ± 0.05 Å	0.08 Å
d_2	1.95 Å	1.99 ± 0.05 Å	—
$\Delta z_{\text{LaO-2}}$	0.00 Å	0.14 ± 0.07 Å	0.21 Å
d_3	1.95 Å	1.90 ± 0.07 Å	—
$\Delta z_{\text{NiO}_2\text{-2}}$	± 0.05 Å	0.05 ± 0.06 Å	0.03 Å
in-plane Ni-O-Ni bond angle	$164 \pm 2°$	$166 \pm 7°$ (average)	$165 \pm 3°$ (average)
out-of-plane Ni-O-Ni bond angle	$175.2 \pm 0.6°$	$\approx 180°$ (not refined)	—

Figure 3. Table summarizing the numerical parameters of the best-fit surface atomic structure obtained in this work for a 10 ML $LaNiO_3(001)_{pc}$ film, and the results of an earlier COBRA study of the surface of a 3 ML $LaNiO_3(001)_{pc}$ film[12]. Defining the $+z$ direction to be perpendicular to the surface of the film, pointing towards the interior of the film, the surface structures are described in terms of intraplanar bucklings $\Delta z_{\text{LaO-i}} \equiv z_{\text{La-i}} - z_{\text{apO-i}}$ and $\Delta z_{\text{NiO}_2\text{-i}} \equiv z_{\text{Ni-i}} - z_{\text{eqO-i}}$ in the top two monolayers ($i = 1, 2$), and interplanar spacings d_j ($j = 1, 2, 3$) between the centers of adjacent LaO and NiO_2 planes—*e.g.*, $d_1 = \frac{1}{2}(z_{\text{Ni-1}} + z_{\text{eqO-1}}) - \frac{1}{2}(z_{\text{La-1}} + z_{\text{apO-1}})$. The leftmost column of the table lists the intralayer bucklings and interplanar spacings reported in Ref. 22 for the bulk of epitaxial thin films of $LaNiO_3$ coherently strained to $LaAlO_3$. The drawings in panels (a) and (b) graphically represent how (b) the best-fit structure obtained by LEED-$I(V)$ analysis compares with (a) the bulk results; the LaO and NiO_2 intraplanar bucklings have been exaggerated in (b) by scale factors of two and four, respectively, for ease of visualization.

an indirect signature of static disorder associated with less than full occupation of these atomic sites. Although the average t-matrix approximation can in principle be used in LEED-$I(V)$ simulations to compute the impact of randomly distributed point defects (including replacements of atom by vacancy) on $I(V)$ curves, we did not pursue this approach in this work because of the low sensitivity of $I(V)$ curves to substitutional disorder, and also because of the introduction of additional parameters into the theory-experiment comparison that such a model would require.

Focusing on the actual values of the refined atomic positions (*cf.* Fig. 3), our *in situ* LEED-$I(V)$ results for the surface structure of our 10 ML $LaNiO_3$ film/$LaAlO_3$ agree quantitatively with the results of COBRA of *ex situ* surface x-ray diffraction data reported previously for LaO-terminated films consisting of 3 ML $LaNiO_3/LaAlO_3$[12]. None of the discrepancies between the two measurements are statistically significant, all lying well within the error bars of the two techniques. The agreement of these two separate experiments, conducted under different measurement conditions on films of different total thicknesses, strongly suggests that the large observed distortions of the near-surface LaO layers are an intrinsic, robust feature of the polar $(001)_{pc}$ surface of $LaNiO_3$.

Furthermore, the intimate coupling between atomic structure and low-energy electronic properties in rare-earth nickelates implies that modifications of the surface electronic structure should occur concomitantly with the dramatic changes in the surface atomic structure of the sort studied in this work. Indeed, Refs. 12 and 28 demonstrate that, *e.g.*, the capping of an ultrathin LaO-terminated $LaNiO_3$ film with an additional NiO_2 layer can "switch" the film from showing metallic to insulating electrical transport behavior. Direct observation of these effects by a surface-sensitive spectroscopic probe such as angle-resolved photoemission spectroscopy (ARPES) would be ideal and represents an intriguing topic for future research.

V. CONCLUSIONS

The strong structure-property relationships in quantum materials provide an ideal knob to control their emergent electronic and magnetic properties through avenues such as epitaxial strain or interfacial engineering, particularly at their surfaces or in atomically thin films. This necessitates *in situ* characterization techniques capable of resolving atomic-scale structural distortions at the surface in order to complement the insights gained into their low-energy electronic structure provided by tools such as ARPES and scanning tunneling microscopy. Here, we employed LEED-$I(V)$ to investigate the surface atomic structure of pristine, MBE-grown thin films of the correlated nickelate $LaNiO_3$ on $LaAlO_3$. Our work identifies large bucklings of the topmost LaO layers within the screening length, consistent with the need for a polar reconstruction along the $(001)_{pc}$ direction, and also

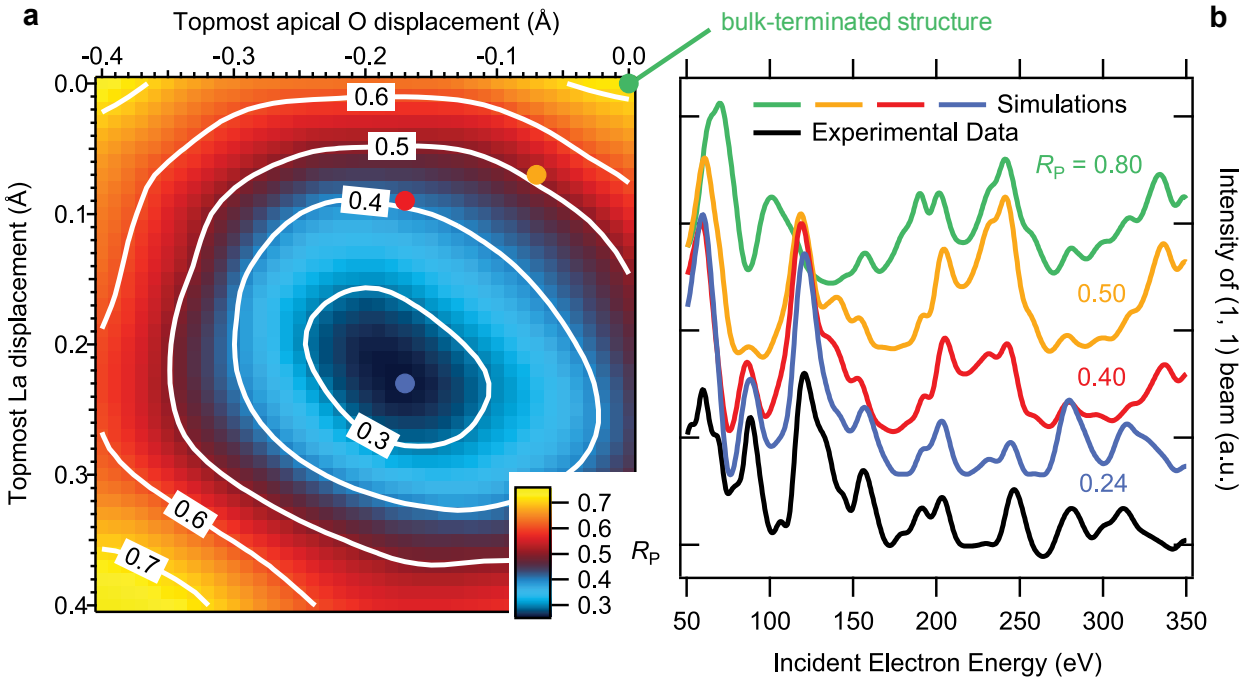

Figure 4. (a) False-color contour plot of the total Pendry reliability factor R_P plotted against displacements of the topmost La and apical oxygen atoms away from the positions they would occupy in a bulk-truncated structure. Positive displacement is defined to be towards the interior of the film; thus proceeding along diagonal line cuts from the upper right to lower left (lower right to upper left) is equivalent to increasing the intraplanar buckling $\Delta z_{\mathrm{LaO\text{-}1}}$ at fixed interplanar spacings d_1 (increasing d_1 at fixed $\Delta z_{\mathrm{LaO\text{-}1}}$). (b) Simulated $I(V)$ curves for the (1,1) beam for four hypothetical structures indicated on the plot in (a) by the four differently colored dots, offset vertically for clarity. The R_P values for just the (1,1) beam are listed next to each curve, which correspond to structures with total R_Ps on the plot in (a) of 0.71 (green, bulk), 0.51 (orange), 0.41 (red), and 0.26 (blue, best-fit).

in excellent quantitative agreement with prior results obtained experimentally by COBRA of surface XRD data and theoretically by density-functional structural relaxation calculations. We expect the phenomena reported here to be general features of complex oxide thin films terminated along nominally polar directions of the underlying crystal structures, and demonstrates its potential as an important tool for engineering orbital polarizations and emergent electronic phases in ultrathin films of quantum materials.

ACKNOWLEDGEMENTS

This work was supported by the Office of Naval Research (grant no. N00014-12-1-0791), and made use of the Cornell Center for Materials Research Shared Facilities, which are supported through the NSF MRSEC program (DMR-1120296). J.P.R acknowledges support from the NSF IGERT program (DGE-0903653). V.B.N acknowledges support from the FAPEMIG (MG/Brazil) UNIVERSAL program (APQ-01961-14). The authors thank C. H. Ahn and D. P. Kumah for discussions.

[1] S. Nakatsuji and Y. Maeno, Physical Review Letters **84**, 2666 (2000).
[2] J. L. García-Muñoz, J. Rodríguez-Carvajal, P. Lacorre, and J. B. Torrance, Physical Review B **46**, 4414 (1992).
[3] Y. Tokura and N. Nagaosa, Science **288**, 462 (2000).
[4] B. Burganov, C. Adamo, A. Mulder, M. Uchida, P. King, J. Harter, D. Shai, A. Gibbs, A. Mackenzie, R. Uecker, M. Bruetzam, M. Beasley, C. Fennie, D. Schlom, and K. Shen, Physical Review Letters **116**, 197003 (2016).

[5] J. Chakhalian, J. M. Rondinelli, J. Liu, B. A. Gray, M. Kareev, E. J. Moon, N. Prasai, J. L. Cohn, M. Varela, I. C. Tung, M. J. Bedzyk, S. G. Altendorf, F. Strigari, B. Dabrowski, L. H. Tjeng, P. J. Ryan, and J. W. Freeland, Physical Review Letters **107**, 116805 (2011).

[6] A. Frano, E. Schierle, M. W. Haverkort, Y. Lu, M. Wu, S. Blanco-Canosa, U. Nwankwo, A. V. Boris, P. Wochner, G. Cristiani, H. U. Habermeier, G. Logvenov, V. Hinkov, E. Benckiser, E. Weschke, and B. Keimer, Physical Review Letters **111**, 106804 (2013).

[7] H. Zhou, Y. Yacoby, V. Y. Butko, G. Logvenov, I. Božović, and R. Pindak, Proceedings of the National Academy of Sciences **107**, 8103 (2010).

[8] K. Zou, S. Mandal, S. D. Albright, R. Peng, Y. Pu, D. Kumah, C. Lau, G. H. Simon, O. E. Dagdeviren, X. He, I. Božović, U. D. Schwarz, E. I. Altman, D. Feng, F. J. Walker, S. Ismail-Beigi, and C. H. Ahn, Physical Review B **93**, 180506 (2016).

[9] I. K. Robinson and D. J. Tweet, Reports on Progress in Physics **55**, 599 (1992).

[10] J. B. Pendry, *Low energy electron diffraction: the theory and its application to determination of surface structure* (Academic Press, London; New York, 1974) oCLC: 1093141.

[11] M. A. Van Hove, W. H. Weinberg, and C.-M. Chan, *Low-Energy Electron Diffraction*, edited by G. Ertl and R. Gomer, Springer Series in Surface Sciences, Vol. 6 (Springer Berlin Heidelberg, Berlin, Heidelberg, 1986).

[12] D. P. Kumah, A. Malashevich, A. S. Disa, D. A. Arena, F. J. Walker, S. Ismail-Beigi, and C. H. Ahn, Physical Review Applied **2**, 054004 (2014).

[13] J. W. Harter, L. Maritato, D. E. Shai, E. J. Monkman, Y. Nie, D. G. Schlom, and K. M. Shen, Physical Review Letters **109**, 267001 (2012).

[14] J. W. Harter, L. Maritato, D. E. Shai, E. J. Monkman, Y. Nie, D. G. Schlom, and K. M. Shen, Physical Review B **92**, 035149 (2015).

[15] P. D. C. King, H. I. Wei, Y. F. Nie, M. Uchida, C. Adamo, S. Zhu, X. He, I. Božović, D. G. Schlom, and K. M. Shen, Nature Nanotechnology **9**, 443 (2014).

[16] A. Mayer, H. Salopaasi, K. Pussi, and R. D. Diehl, Computer Physics Communications **183**, 1443 (2012).

[17] A. Barbieri and M. A. Van Hove, "Symmetrized automated tensor leed package, available from m. a. van hove,".

[18] J. Rundgren, Physical Review B **68**, 125405 (2003).

[19] The energy dependence of the inner potential phenomenologically accounts for dynamical screening of the LEED signal electron by an exchange-correlation hole as they propagate through the solid.

[20] V. B. Nascimento, R. G. Moore, J. Rundgren, J. Zhang, L. Cai, R. Jin, D. G. Mandrus, and E. W. Plummer, Physical Review B **75**, 035408 (2007).

[21] R. G. Moore, V. B. Nascimento, J. Zhang, J. Rundgren, R. Jin, D. Mandrus, and E. W. Plummer, Physical Review Letters **100**, 066102 (2008).

[22] S. J. May, J.-W. Kim, J. M. Rondinelli, E. Karapetrova, N. A. Spaldin, A. Bhattacharya, and P. J. Ryan, Physical Review B **82**, 014110 (2010).

[23] R. Matzdorf, Ismail, T. Kimura, Y. Tokura, and E. W. Plummer, Physical Review B **65**, 085404 (2002).

[24] J. B. Pendry, Journal of Physics C: Solid State Physics **13**, 937 (1980).

[25] Y. F. Nie, Y. Zhu, C.-H. Lee, L. F. Kourkoutis, J. A. Mundy, J. Junquera, P. Ghosez, D. J. Baek, S. Sung, X. X. Xi, K. M. Shen, D. A. Muller, and D. G. Schlom, Nature Communications **5** (2014), 10.1038/ncomms5530.

[26] J. H. Lee, G. Luo, I. C. Tung, S. H. Chang, Z. Luo, M. Malshe, M. Gadre, A. Bhattacharya, S. M. Nakhmanson, J. A. Eastman, H. Hong, J. Jellinek, D. Morgan, D. D. Fong, and J. W. Freeland, Nature Materials **13**, 879 (2014).

[27] R. Bliem, E. McDermott, P. Ferstl, M. Setvin, O. Gamba, J. Pavelec, M. A. Schneider, M. Schmid, U. Diebold, P. Blaha, L. Hammer, and G. S. Parkinson, Science **346**, 1215 (2014).

[28] D. P. Kumah, A. S. Disa, J. H. Ngai, H. Chen, A. Malashevich, J. W. Reiner, S. Ismail-Beigi, F. J. Walker, and C. H. Ahn, Advanced Materials **26**, 1935 (2014).